A selective morphosynthetic approach for single crystalline hematite through morphology evolution via microwave assisted hydrothermal synthesis

Chang Woo Kim[a,b], Myung Jong Kang[a], Thanh Khue Van[a,c], Young Soo Kang[a,*]

[a] Korea Center for Artificial Photosynthesis and Department of Chemistry, Sogang University, #1 Shinsu-dong, Mapo-gu, Seoul 121-742, Republic of Korea
[b] Department of Graphic Arts Information Engineering, College of Engineering, Pukyong National University, 365, Sinseon-ro, Nam-gu, Busan 48547, Republic of Korea
[c] Faculty of Chemistry Technology, Industrial University of Ho Chi Minh City (IUH), 12 Nguyen Van Bao St., Ward 4, Go Vap Dist., HCMC, Vietnam

ABSTRACT

Hematite single crystals are one of most promising materials which is able to apply for the field of catalyst industry. Even its prospective applicability, strategies for improving its catalytic performance are still not enough to meet the requirements for industrial application. In the present work, we demonstrate a morphology selective one pot reaction for a hematite single crystal by microwave-assisted hydrothermal synthesis. The microwave-assisted hydrothermal route, taking advance of the exposed crystal facet-based activity of the material, is suggested to crystal facet controlling synthesis of the hematite crystal. The dispersant and capping agents such as sodium carboxymethyl cellulose and N_2H_4, respectively, play a very important role in controlling the exposed crystal facet and morphological uniformity for a selective morphology of hematite crystal. In addition, systematically experimental examination of the well-exposed facet is interestingly giving an insight into the crystal growth and morphological evolution of single crystalline hematite from plate to tetrahexagonal bipyramid, octahedral and oblique cubic shape. Physicochemical techniques were used to characterize and evaluate the photoactivity of the material in detail. In here, a well-defined crystal facet is obtained and expected to be applied as an efficient catalysts and its synthetic methodology is applicable to other metal oxide photocatalyst.

© 2017 The Korean Society of Industrial and Engineering Chemistry. Published by Elsevier B.V. All rights reserved.

Introduction

The urgent requirement for solving the current serious environmental issues and insufficient energy in the world has prompted scientists paying a great attention to research strategies and alternative energy sources [1]. Photo-induced environment treatment and water splitting have been considered as a potential and promising strategy for the environmentally-friendly. Since TiO_2 was used as photocatalyst in 1972 at first for water splitting, semiconducting photocatalysts have been significantly studied and researched for its enhancing photocatalytic performance [2]. Considering a high light absorption ability which is attributed to the high photocatalytic activity, environmentally friendly, low cost processing, renewability, and high productivity, semiconducting transition metal oxides have exhibited great promising potentials for the field of catalyst industry [3]. Especially, together with consideration that the physical and chemical properties of semiconducting transition metal oxide photocatalysts depend on the morphology and crystal structures [4], because of surface area, crystal surface energy and particle size as well, hematite (α-Fe_2O_3), one of the most abundant semiconductor materials, is the most prospective material for photocatalyst industry among various semiconducting transition metal oxide photocatalysts [5].

Hematite is widely used in various applications such as pigments, batteries, absorbents, catalysts, etc. [6–11]. Hematite, n-type semiconductor, possesses an optimal optical indirect band gap transition [12,13] (Eg = 2.1 eV) which is capable of absorbing light up to 600 nm, be thermodynamic stability in oxidative environment, nontoxicity, and low processing cost. However, there are also many limitations in pristine hematite to be used practically

as high performance photoanodes that challenge ones to overcome such as short charge diffusion length, L_D ($\sim$2–4 nm) [13], low mobility of the minority charge carriers (0.2 cm^2 V^{-1} s^{-1}) [14] which are resulting in high electron and hole recombination rate ($<$ 10 ps) [15], high resistance [16] and sluggish kinetics of oxygen evolution (OER) [17]. Over the last few decades, morphology controlled synthesis of single crystal nanoparticles has significantly devoted insights into the crystal evolution and the superiority of materials in terms of physiochemical properties [18]. Such as, a large quantity of fairly uniform rhombohedral crystals obtained from solution of HCl and Fe(NO)$_3$ at around 100 °C [6], α-Fe$_2$O$_3$ nanoparticles by adjusting the polarity of the mixed solvent [19], hematite nanorod array photoanodes through hydrothermal route and post heat treatment [20], numerous strategies in hematite structuring have been devoted to improve the efficiency and practical use as well [21–23]. Moreover, hematites have shown synergetic effects as a composite material which was junctioned with TiO$_2$, BiOI and g-C$_3$N$_4$ [24–27].

Interestingly, a research on a hole-transfer kinetic at the interface by Klahr et al. [28] reveals new insight on the photocurrent and efficiency for water splitting [28] and Yu and co-worker also demonstrated facet-dependant photocatalytic properties on photocatalyst [29–31]. In our previous work, hematite single crystal from truncated hexagonal bipyramid (THB) to cube shape has successfully shown interesting photo-catalytic performance [32]. Till date, even that much effort has been devoted to control morphology of hematite materials via various approaches, specific morphology of hematite single crystal was just synthesized under individual reaction condition. As such, its morphology selectivity in the one pot reaction has been rarely reported in hematite structuring.

In the current report, we demonstrate a morphology selective one pot reaction for a hematite single crystal by microwave-assisted hydrothermal synthesis. With microwave-assisted hydro-thermal system, which convert water molecules to be exited to high energy state and do accelerating the reactions [33], a uniform hematite single crystal enclosed with various crystal facets were synthesized and resulted in high productivity. The hematite particle shape evolution from oblique cubic to octahedron of morphosynthetic approach and role of reactants used are explored. Morphology controlled hematite single crystal are characterized and analyzed for facet dependent properties in detail. It is considered that surface energy of the crystal facet is attributed to the photoactivity of the hematite single crystal. The photo-activity of the hematite nanoparticles exposing different facets was evaluated through photo-degradation of rhodamine B (RhB). It is expected that a morphosynthetic approach through a selective

morphology evolution is able to be applied for catalyst industry and its synthetic methodology is applicable to other metal oxide photocatalyst.

Experimental

Materials and reagents

All the reagents were AR grade and used in the synthetic experiments without any further purification, unless otherwise mentioned. Hydrazine hydrate solution (N$_2$H$_4$·xH$_2$O, 60%), sodium carboxymethyl cellulose (CMC, Mw = 250,000), potassium hex-acyanoferrate(III) (K$_3$[Fe$_3$(CN)$_6$]) were all purchased from Aldrich commercial source. High purity distilled deionized water (DDW) (resistivity > 18 MΩ) was used as solvent for preparing the reaction solutions of the experiments.

Microwave-assisted hydrothermal synthesis

In a typical synthetic methodology, hematite nanocrystal were synthesized by mainly following our previous published work getting along with a microwave system [32,34]. A mixture of 20 mL solution of K$_3$[Fe$_3$(CN)$_6$] (0.01 M), CMC (3.5 g L^{-1}) and N$_2$H$_4$ (1.5%) was prepared and stirred for 30 min with electromagnetic stirrer. Then, the reaction solution was transferred into a microwave reactor's vessel. The microwave-assisted hydrother-mal synthetic treatment was performed at 160 °C for 1 h in a microwave reactor (CEM MARS 230/60 907501 MICROWAVE ACCELERATED REACTION SYSTEM, CEM corporation in USA). After carrying out the reaction process, the reaction was allowed cooling down naturally to room temperature. All of the synthesized products were washed by centrifuging repeatedly with absolute ethanol, distilled deionized water and subsequent-ly dried at 80 °C in ambient condition. Variation of precursor concentration (K$_3$[Fe$_3$(CN)$_6$]) in other experiments was carried out in the same procedure to obtain the different shapes of the hematite particles.

Photocatalytic activity measurement

Reaction of photocatalytic degradation of dyes Rhodamine (RhB) were carried out at room temperature under the irradiation of 1 sun lamp 2.5 W. The as-synthesized hematite nanocrystal (30 mg) were dispersed into 50 mL RhB aqueous solution which was dissolved into DI water of 10 mg L^{-1}. The changes of the optical property for the dye are recorded on the Shimadzu UV-310PC UV–vis absorption spectrophotometer over the range from 200 to
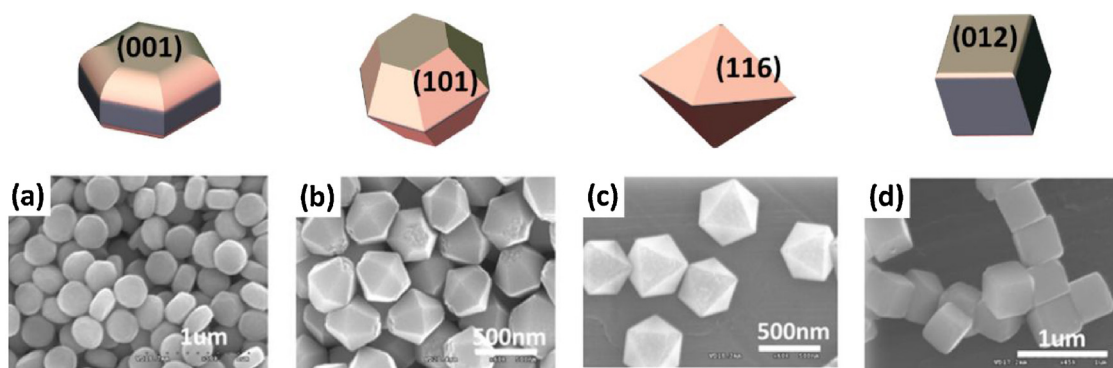
Scheme 1. Morphologically well faceted evolution of hematite nanocrystal from plate-truncated hexagonal bipyramid (THB, (a)), THB (b), to octahedral (c) and oblique cubic (d) morphology.
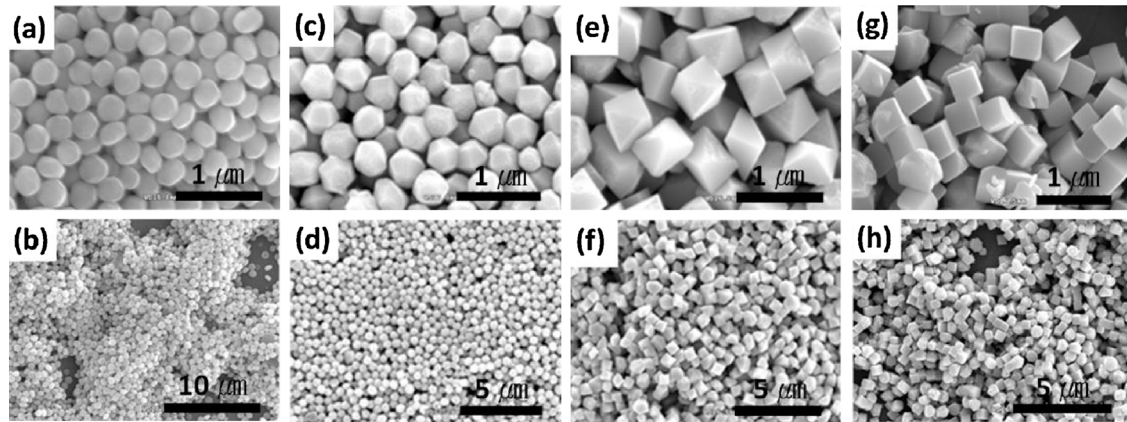
Fig. 1. Morphological evolution of hematite crystals in SEM image; Plate-THB (a, b), THB (c, b), octahedral (e, f) and oblique cubic (g, h) shape.

800 nm after centrifugation to eliminate the suspended hematite nanocrystal in the RhB solution.

Characterization technique

Morphology and crystal structure as well as chemical compositions of the as-synthesized products were analyzed by scanning electron microscopy (SEM (Hitachi S-4300 FE-SEM)) and transmission electron microscopy (TEM) with JEM 2100F (JEOL) equipped with EDX operated at accelerated at 200 kV. In a brief procedure for sampling of SEM and TEM analyzing, the as-fabricated α-Fe$_2$O$_3$ nanocrystal were dispersed in ethanol solution by sonication agitation for a while. A drop of the dispersant-solution sample was released on the SEM holder and dried at 80 °C in ambient condition and then coated with Pt for 90 s. Similarly, a drop of dispersant-solution sample was released on carbon-enhanced copper grids and dried at 80 °C in ambient condition for TEM checking. The crystal structure of the as-synthesized product was characterized by X-ray diffraction on a Rigaku miniFlex-II desktop X-ray diffractometer, Cu Kα radiation with $\lambda = 0.154056$ nm. The diffraction patterns were recorded in the 2θ range from 20 to 80 with step size of 0.02° at 2°/min. UV–vis spectra of the as-synthesized powder were measured at room temperature in air on a Shimadzu UV-310PC over the range from 200 to 800 nm. Surface area of the sample powders was analyzed from Brunauer, Emmett and Teller (BET) method at 77 K and the nitrogen adsorption–desorption isotherm curves using Autosorb-1 Quantachrome Instrument.
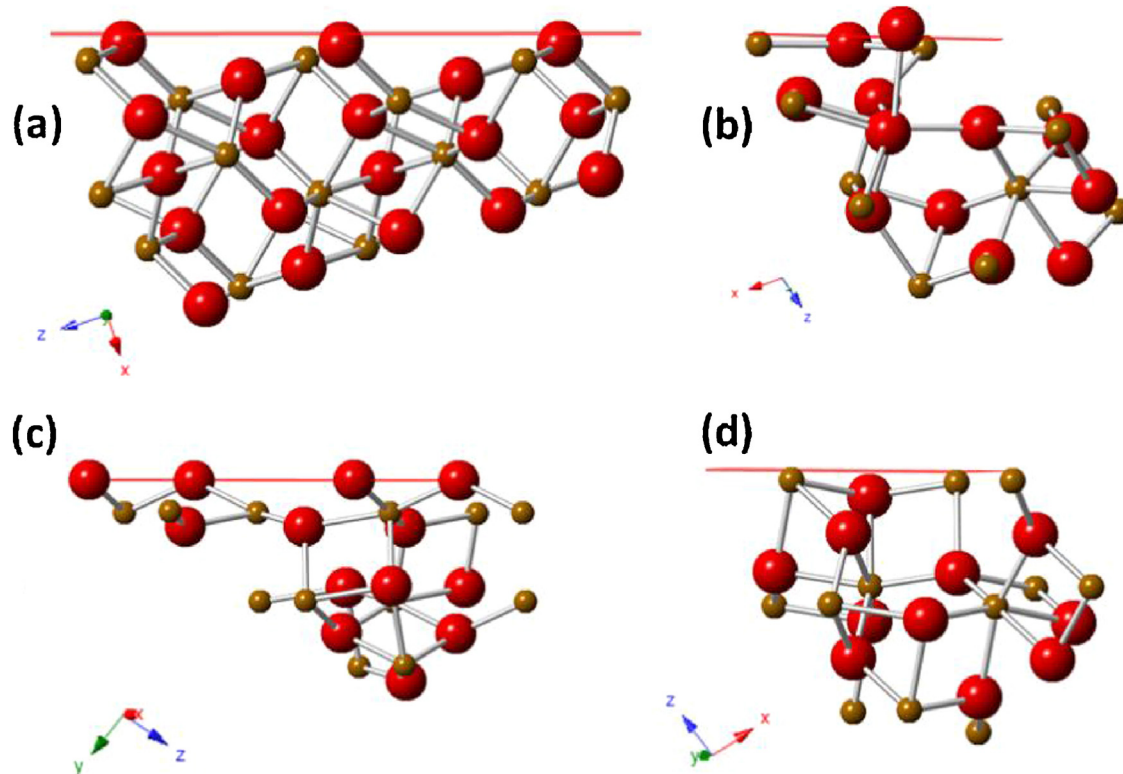

Fig. 2. Atomic arrangement of exposed facets in hematite nanocrystal; a (101) facet (a), a (116) facet (b), a (104) facet (c) and a (012) facet (d).
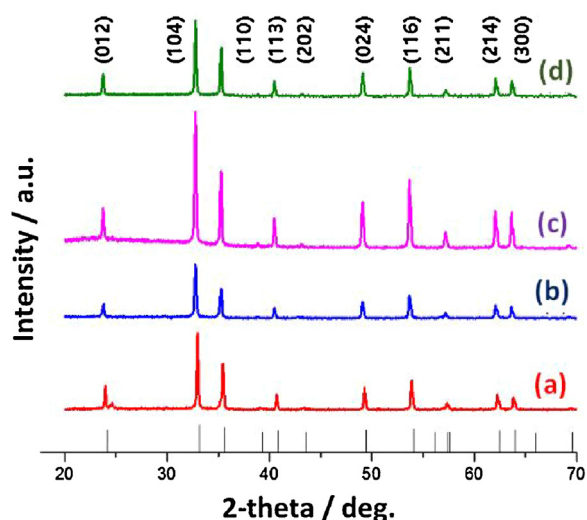
Fig. 3. Morphological evolution of hematite crystals in XRD spectra; Plate-THB (a), THB (b), octahedral (c) and oblique cubic (d) shape.

Results and discussion

Facet engineering of single crystalline semiconducting materials is highly related with their surface energy [35]. Considering the fact that their overall surface energy should be lowest, it tends to expose the facets with the lowest surface energy. Even though the exposure of unique facet with high miller index is energetically unfavourable, recent reports have shown that structure directing agent such as dispersant and capping agents help to stabilize unfavourable facets by deactivating their high surface energy. And it result in ultimately exposing these unique facets in the single crystal structure. In the current work, we report microwave-assisted hydrothermal synthesis to tailor the hematite nanocrystals with uniformly and dominantly specific (101) crystal facet using sodium carboxymethyl cellulose (CMC) and hydrazine (N_2H_4) as dispersant and capping agent, respectively. Based on our previous work [32,34,36], a microwave-assisted hydrothermal route was applied as an advanced study on the morphological controlling synthesis. Considering the fact that the specific polarity

of solvent molecules is interacted with microwave, the polar solvent molecules absorb microwave which convert them to be exited to a high energy state and result in accelerating the reactions in the polar medium [33].

With the help of a microwave radiation, the chemical reaction goes more rapidly and homogeneously in polar solvent. Its synthetic methodology is beneficial for the uniformity of the crystal growth and saving energy in the view of catalyst industry [34]. For example, facet controlled single crystal was achieved under 1 h in our approach, compared that conventional hydrothermal route require over 8 h of reaction time. Strikingly the as-synthesized α-Fe_2O_3 crystal products were produced with good uniformity in size and shape and selectively well-faceted in a microwave-assisted hydrothermal synthesis. Interestingly, when the concentration of iron precursor, $K_3[Fe_3(CN)_6]$, was decreased from 0.02 M to 0.015 M, 0.01 M, and 0.008 M while the concentration of N_2H_4 and CMC were kept constant at 1% and 3.5 g L^{-1}, respectively, the morphological evolution of as-synthesized hematite nanocrystals takes place from plate-THB (Scheme 1a) to THB (Scheme 1b), octahedral (Scheme 1c) and oblique cubic (Scheme 1d) shape in high uniform regime as demonstrating in the Scheme 1 being along with representative scanning electron microscopy (SEM) images. Crystal structure of hematite tends to grow along with crystallographically equivalent direction to form dendritic shape [32]. CMC molecules have an effect on isotropic growth of hematite structure for spherical shape [32]. Based on the crystallographic structure of hematite in the Scheme 1, the presence of CMC and N_2H_4 as a structure directing agent guides α-Fe_2O_3 seed particle to get the anisotropic growth with six directions of equivalent plane {100} and two other directions of equivalent planes {001}, and finally results in the plate-THB (Scheme 1a) and THB particle shapes (Scheme 1b). The assistance of microwave irradiation accelerates whole hydrothermal reaction to be homogeneous condition which is responsible for well growing of the crystals as compared with only using the hydrothermal route. It results that THB shaped nanocrystal was successively formed even less molar concentration of iron precursor was involved to 0.015 M from 0.02 M as compared with the singular hydrothermal approach. Interestingly, octahedral and oblique cubic nanocrystal was synthesized in Scheme 1(c) and (d) when the concentration of iron precursor was decreased to 0.01 M,
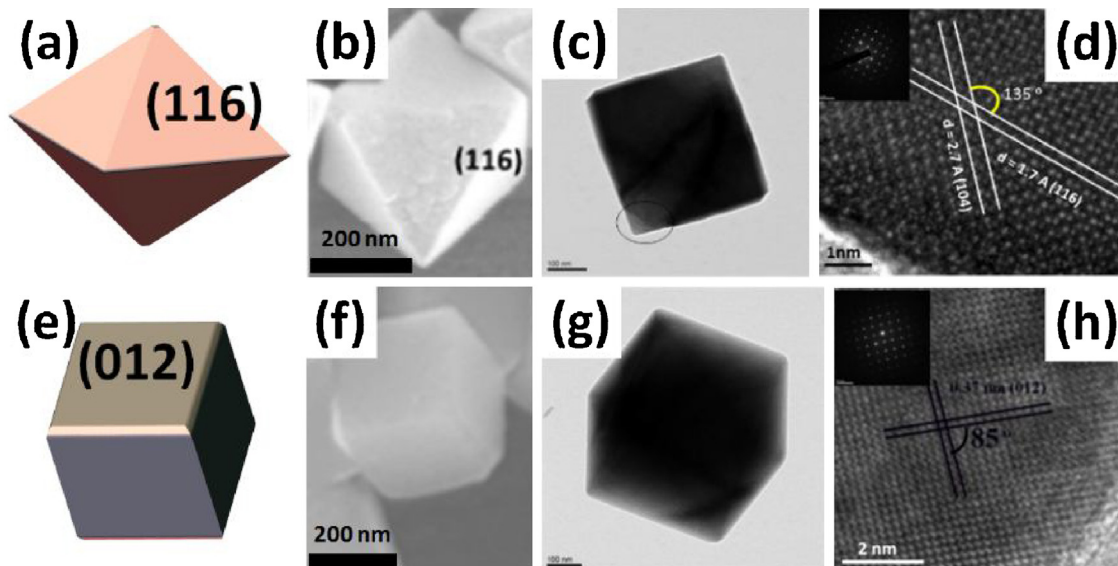

Fig. 4. Scheme, SEM and TEM images of typical hematite particles of octahedral and cubic shape; Geometrical model (a), SEM image (b), TEM image (c), HRTEM and SAED pattern (d) of the octahedral hematite particle. Geometrical model (e), SEM image (f), TEM image (g), HRTEM and SAED pattern (h) of the hematite cubic crystal.
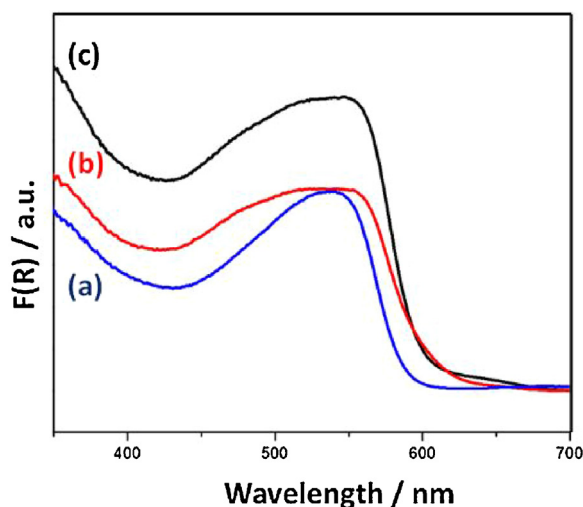
Fig. 5. UV–vis spectra of THB (a), octahedral (b) and oblique cubic (c) shape of hematite crystals.

and 0.008 M, respectively. The morphologies of hematite nanocrystal was examined with SEM observation in Scheme 1 and Fig. 1. Typical SEM images of hematite nanocrystals depending on the molar concentration between iron precursors and structure directing agent were presented in Fig. 1. Fig. 1(a) and (b) shows representative SEM images of plate-THB when 0.018 M of iron precursor was involved under a microwave-assisted hydrothermal approach. As shown in representative SEM images (Fig. 1c and d), as-synthesized hematite nanocrystals are quite uniform and well-faceted with ca. 400 nm of nanocrystal when molar concentration of iron precursor was decreased to 0.015 M. As a concentration of $K_3[Fe_3(CN)_6]$ was decreased from 0.015 M to 0.01 M, and 0.008 M, the hematite nanocrystal shape evolves from THB shape to octahedron (Fig. 1e and f) and oblique cubic (Fig. 1g and h), respectively. Fig. S1 in the Supporting information reveals that the

as-synthesized hematite nanocrystals in larger scale are uniform in size and shape. As the molar concentration of $K_3[Fe_3(CN)_6]$ was decreased, molar concentration of structure directing agent like hydrazine is increased so that it becomes to be adsorbed onto the specific surface of the hematite seed particle selectively. Interestingly the increased concentration of hydrazine induced a (101) of THB, a (116) of octahedron and a (012) of oblique cubic. Hydrazine-induced facets were characterized in a crystallographic aspect as shown in Fig. 2. Fig. 2 shows different atomic arrangement in each exposed facet of hematite nanocrystal. Specific atomic arrangement come from dangling bond in the top-most layer of surface as shown in Figs. 2 and S2. As such, their unique dangle bond of exposed facets contribute surface energy. Consequently, the morphology-engineered nanocrystal produces the high surface energetic facets. In the hematite nanocrystal under a microwave-assisted hydrothermal synthesis, octahedral shape is enclosed with {104} and {116} and oblique cubic shape is enclosed with {104} and {012}, respectively. The theoretical calculation on surface energy demonstrates that the (012), (110), (104) and (100) facets of hematite nanocrystal possess surface energies as $11.35\,J\,m^{-2}$, $4.0279\,J\,m^{-2}$, $1.605\,J\,m^{-2}$ and $1.003\,J\,m^{-2}$, respectively [37]. It indicates that hydrazine is adsorbed onto the specific surface and stabilizes a high energetic surface of hematite nanocrystal.

Hydrazine-induced crystal structure of hematite nanocrystal was characterized by X-ray powder diffraction (XRD) in Fig. 3. All of the identified diffraction peaks are perfectly indexed to the hexagonal with cell constants $a = b = 0.50356\,nm$ and $c = 1.37489\,nm$ α-Fe_2O_3 phase (JCPDS card no. 33-0664; space group $R\bar{3}c$ (#167)). The strong and narrow sharp diffraction peaks of all the samples indicate that all the as-synthesized hematite nanocrystals are high crystalline. There are no other structural features of impurities detected in the samples.

To clarify the crystal-faceted structure as well as the single crystal of hematite nanocrystal, typically TEM, HRTEM and SEAD pattern analysis for the octahedral and oblique cubic crystals was studied and presented in Fig. 4. The octahedral crystal is enclosed
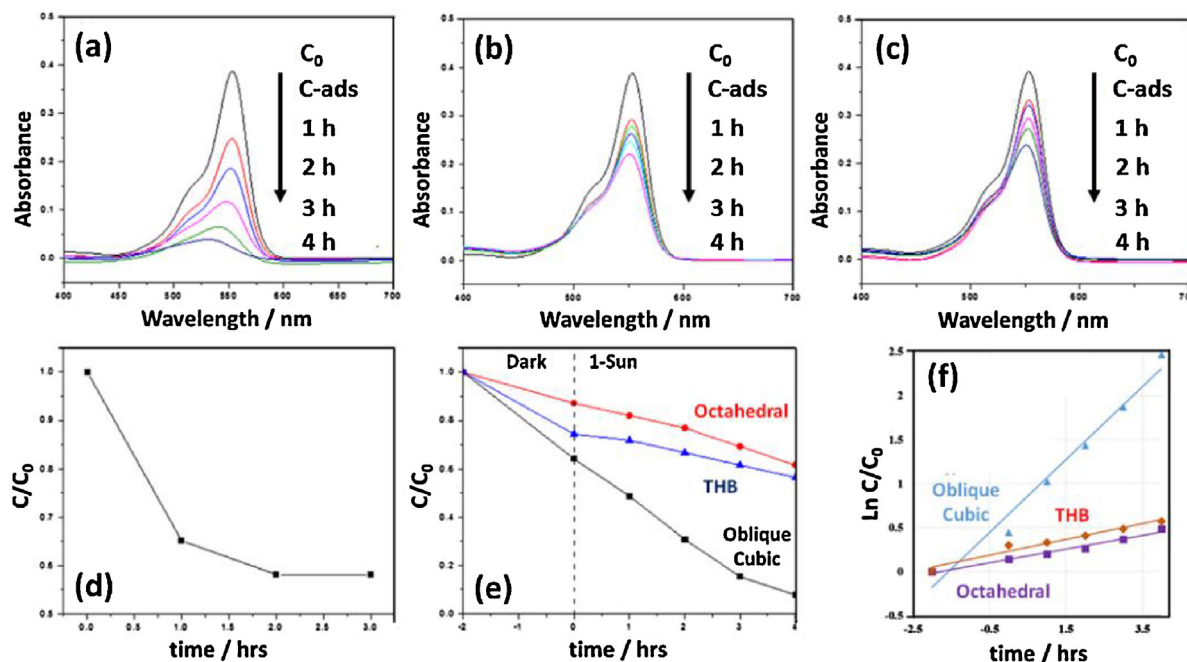

Fig. 6. UV–vis optical absorption spectra on the photocatalytic degradation of RhB in the presence of hematite nanocrystal; (a) cubic, (b) THB, (c) octahedral shape. The RhB adsorption curve versus time in the presence of oblique cubic nanocrystal under dark condition (d). Photodegradation curves of RhB versus photoirradiation time in the presence of hematite nanocrystals with different morphologies under illumination (e) and pseudo-first-order degradation rate constants of RhB (f).
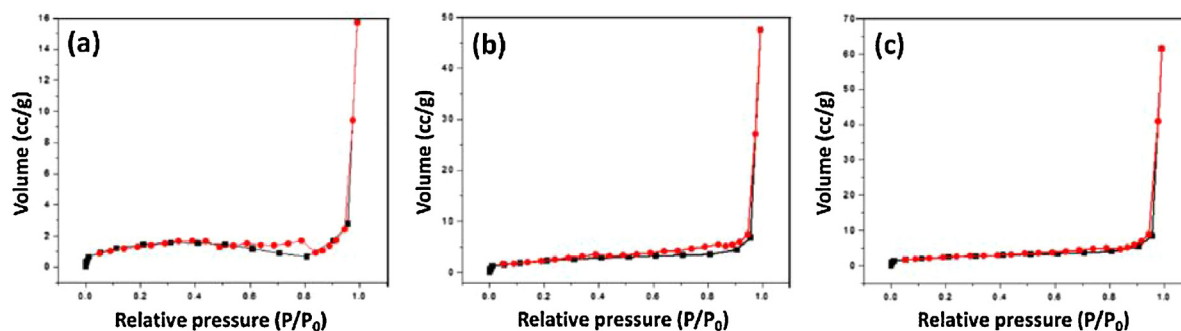
Fig. 7. N$_2$ adsorption/desorption BET isotherm curves of the hematite nanocrystals; cubic (a), THB (b) and octahedral (c) shape. Black line; adsorption, red line; desorption. (For interpretation of the references to color in this figure legend, the reader is referred to the web version of this article.)

by four {116} crystal facets and four others {104} crystal facets which are consisted with the geometrical model as presenting in Fig. 4(a) and (b). Representative TEM and HRTEM images of octahedral crystal was presented in Fig. 4(c) and (d). In the octahedral structure, a lattice distance was observed 1.7 Å and 2.7 Å which was indexed as (116) and (104), respectively. SAED pattern from HRTEM image indicates well-exposed crystal facet of hematite single crystal. EDX mapping image and spectra of octahedral hematite nanocrystal is shown in Fig. S3. Typical oblique cubic structure is enclosed by two {104} crystal facets and four others {012}, which is consisted with the geometrical model as presenting in Fig. 4(e) and (f). In Fig. 4(g) and (d), TEM and HRTEM image of oblique cubic structure show that 3.7 Å was indexed as (012). The SEAD patterns presented in the inset indicate that the hematite crystals are all perfect single crystalline. For the tetrahexagonal bipyramid shaped particles (THB) in Figs. 1 and S1 (b), a detailed characterization with TEM as well as SEM were shown as our previous report [32]. THB shaped particle is enclosed by 12 highly symmetric side-trapezoidal facets corresponding to the probably Miller indices (101), (011), (1$\bar{1}$1), ($\bar{1}$01), ($\bar{1}$11), and (0$\bar{1}$1) and (10$\bar{1}$), (01$\bar{1}$), (1$\bar{1}\bar{1}$), ($\bar{1}$0$\bar{1}$), ($\bar{1}$1$\bar{1}$), and (0$\bar{1}\bar{1}$) and two facets at top and bottom could be indexed as (001) and (00$\bar{1}$), respectively. For the plate-THB shaped particles, the facets are just similar to the THB particle unless their {001} facets are more enlarged than that of the THB particle.

For better understanding of the exposed crystal facet, the optical properties of as-prepared hematite nanocrystal was characterized by UV–vis spectroscopy as shown in Fig. 5. Three kinds of nanocrytals exhibit distinct optical properties of hematite nanocrystal in UV–vis spectra. Interestingly the dominant crystal facet of hematite nanocrystal reveals different onsets of visible absorption in Fig. 5. The onset of visible absorption of THB crystal was observed at 610 nm in Fig. 5(a). Octahedral nanocrystal exhibits the onset of visible absorption at 660 nm in Fig. 5(b) compared with the result that the onset of visible absorption is at 650 nm in the oblique cubic nanocrystal (Fig. 5c). The difference of onset absorption between representative three kinds of nano-crystals come from the ratio between specific facets. Especially the existence of {104} facet makes a difference of onset wavelength between THB and octahedral, oblique cubic nanocrystals. Com-pared with that of THB nanocrystal, the onsets of visible absorption of the octahedral and oblique cubic crystals are almost similar because there are almost similar exposed crystal facets {104} appearing in their surface. As expected, dominantly exposed certain crystal facet of semiconductor nanoparticles could exhibit distinct physicochemical properties. Based on optical properties of UV–vis spectra, the photocatalytic activity of the as-synthesized hematite nanocrystal was examined via photo-catalytic

degradation of the organic compounds. The photocatalytic activity of hematite nanocrystal was compared with oblique cubic (Fig. 6a), THB (Fig. 6b) and octahedral shape (Fig. 6c). Before photo-degradation experiment, three kinds of hematite nanocrystals were aged into dye-molecules for dye-adsorption onto the surface of nanocrystal under dark condition. In Fig. 6(a)–(c), decrease of dye concentration from C$_0$ to C-ads come from initial adsorption of dye molecules on the surface of nanocrystal. Fig. 6(d) shows the RhB adsorption curve versus time in the presence of oblique cubic nanocrystal under dark condition. It indicates that concentration of dye molecules was not decreased after 2 h. Even three kinds of hematite nanocrystal show different adsorption ability under dark condition, it is related with atomic arrangement of each facet, which was exposed on nanocrystal. Because each hematite naoncrystal shows different chemical bonding site for adsorption of RhB-dye molecules based on Fig. 2. After complete dye-adsorption onto the surface of nanocrystal, dye-hematite solution was illuminated and concentration of dye-molecules was recorded as a function of time in Fig. 6(e). It indicates that oblique cubic hematite nanocrystal show the highest rate of photodegradation compared with that of THB and octahedral nanocrystal. It indicates that the rate of photodegradation of dye-RhB is critically affected by the crystal shape exposing specific facets. Considering that the photocatalytic reaction occurs on the surface of photocatalyst, the energetics on the surface depends on specific facet with unique surface energy. Accordingly, the surface energy of {012} facets which are mainly dominating from the oblique cubic-shaped nanocrystal is highest. From the photocatalytic test of RhB, the results of photocatalytic activity of the hematite nanocrystals are consisting with the theoretical calculation in the surface energy of the crystals point of view. Thereby, the rate of photodegradation of dye-RhB is highest for the oblique cubic shape. And for the octahedral and THB shape the rate is relatively lower. To estimate the kinetic parameters of RhB dye degradation (k and n), an nth-order kinetic equation is described by the relation:

$$\text{rate}_{dye} = -dC/dt = kC^n$$

The first-order kinetic model (n = 1) is simplified:

$$-\ln C/C_0 = kt$$

where rate$_{dye}$ is the degradation rate of the RhB (mg min^{-1}), C and C$_0$ are the actual and initial concentrations of the dye (mg L^{-1}), respectively, t is the illumination time, k is the photo degradation rate constant (1 min^{-1}). Fig. 6(f) shows the ln C/C$_0$ of the dye as a function of irradiation time for the oblique cubic-, octahedral- and THB-shaped hematite nanocrystals. As it clearly reveals that reduction of the dye concentrations follows a linear pattern toward the exposed time for the various facet-shaped crystals. This

indicates that the photodegradation of the RhB dye obeys the rules of a pseudo-first-order kinetic reaction.

The photocatalytic activity depends also on the specific surface area of photocatalyst. The Brunaure, Emmett, and Teller (BET) technique was applied to characterize the specific surface area of hematite nanocrystal. Fig. 7 shows N_2 adsorption/desorption isotherm curves of hematite nanocrystal with cubic, THB and octahedral shape. All the isotherm graphs show typical behavior of particle-typed powder. The BET surface area of the cubic, octahedral and THB hematite nanocrystal were calculated to be of 6.632 m^2 g^{-1}, 7.901 m^2 g^{-1} and 7.326 m^2 g^{-1}, respectively. It reveals that the specific surface areas of three kinds of nanocrystal are quite similar to each other. It indicates that the diameter of three kinds of nanocrystal shows similar size as characterized in SEM images. As such, the difference of photocatalytic performance comes from specifically exposed facet on the hematite nano-crystals.

Conclusion

In conclusion, we have demonstrated a morphology selective one pot reaction for a hematite single crystal by microwave-assisted hydrothermal synthesis. With microwave-assisted hydro-thermal system, a uniform hematite single crystal enclosed with various crystal facets were synthesized and yielding in high productivity. The synthetic methodology showed a morphology evolution of the hematite crystal from plate THB to THB, octahedral and oblique cubic shape with changing reactant precursor concentrations in one pot. Modern physical characterization had conducted to define clearly the as-synthesized particle sample is pure hematite, single crystalline and defined crystal facets. Examination on the photocatalytic activity of the particle sample has revealed that the oblique cubic particles enclosed with dominantly {012} crystal facets is highest photocatalytic activity compared with the others. This is possibly resulting from the high surface energy of the crystal facets of the particle. The BET characterization and theoretical calculation on surface energy support the result consistently. This must be practical promising clues to the researchers to study and application on the material. It is expected that a morphosynthetic approach through a selective morphology evolution is able to be applied for catalyst industry and its synthetic methodology is applicable to other metal oxide photocatalysts.

Acknowledgements

Appendix A. Supplementary data

Supplementary data associated with this article can be found, in the online version, at http://dx.doi.org/10.1016/j.jiec.2017.05.005.

References

[1] A. Fujishima, K. Honda, Nature 238 (1972) 37.
[2] M.G. Walter, E.L. Warren, J.R. McKone, S.W. Boettcher, Q. Mi, E.A. Santori, N.S. Lewis, Chem. Rev. 110 (2010) 6446.
[3] T.K. Van, L.Q. Pham, D.Y. Kim, J.Y. Zheng, D. Kim, A.U. Pawar, Y.S. Kang, ChemSusChem 7 (2014) 3505.
[4] C. Suryanarayana, Non-Equilibrium Processing of Materials, Pergamon Materials Series, Pergamon Press, New York, 1999.
[5] D.A. Wheeler, G. Wang, Y. Ling, Y. Li, J.Z. Zhang, Energy Environ. Sci. 5 (2012) 6682.
[6] R.M. Cornell, U. Schwertmann, The Iron Oxides: Structure, Properties, Reactions, Occurrences and Uses, Wiley-VCH Verlag, Weinheim, 2003.
[7] A. Khataee, P. Gholami, B. Vahid, J. Ind. Eng. Chem. 50 (2017) 86.
[8] J. Yin, Z. Yu, F. Gao, J. Wang, H. Pan, Q. Lu, Angew. Chem. Int. Ed. 49 (2010) 6328.
[9] X. Mou, X. Wei, Y. Li, W. Shen, CrystEngComm 14 (2012) 5107.
[10] M. Zhu, Y. Wang, D. Meng, X. Qin, G. Diao, J. Phys. Chem. C 116 (2012) 16276.
[11] C. Pojanavaraphan, U. Satitthai, A. Luengnaruemitchai, E. Gulari, J. Ind. Eng. Chem. 22 (2015) 41.
[12] I. Balberg, H.P. Pinch, J. Magn. Magn. Mater. 7 (1978) 12.
[13] J.H. Kennedy, K.W. Frese Jr., J. Electrochem. Soc. 125 (1978) 709.
[14] A.J. Bosman, H.J. Vandaal, Adv. Phys. 19 (1970) 1.
[15] N.J. Cherepy, D.B. Liston, J.A. Lovejoy, H. Deng, J.Z. Zhang, J. Phys. Chem. B 102 (1998) 770.
[16] M.P. Dare-Edwards, J.B. Goodenough, A. Hamnett, P.R. Trevellick, J. Chem. Soc. Faraday Trans. 79 (1983) 2027.
[17] S.D. Tilley, M. Cornuz, K. Sivula, M. Gratzel, Angew. Chem. Int. Ed. 49 (2010) 6405.
[18] L.Q. Pham, T.K. Van, H.G. Cha, Y.S. Kang, CrystEngComm 14 (2012) 7888.
[19] R. Yu, Z. Li, D. Wang, X. Lai, C. Xing, X. Xing, Solid State Sci. 11 (2009) 2056.
[20] Y.-R. Hong, Z. Liu, S.F.B.S.A. Al-Bukhari, C.J.J. Lee, D.L. Yung, D. Chi, T.S.A. Hor, Chem. Commun. 47 (2011) 10653.
[21] Y. Lin, G. Yuan, S. Sheehan, S. Zhou, D. Wang, Energy Environ. Sci. 4 (2011) 4862.
[22] A. Kay, I. Cesar, M. Gratzel, J. Am. Chem. Soc. 128 (2006) 15714.
[23] K. Sivula, R. Zboril, F.L. Formal, R. Robert, A. Weidenkaff, J. Tucek, J. Frydrych, M. Gratzel, J. Am. Chem. Soc. 132 (2010) 7436.
[24] S.-E. Kim, J.-Y. Woo, S.-Y. Kang, B.K. Min, J.K. Lee, S.-W. Lee, J. Ind. Eng. Chem. 43 (2016) 142.
[25] N. Abbas, G.N. Shao, M.S. Haider, S.M. Imran, S.S. Park, H.T. Kim, J. Ind. Eng. Chem. 39 (2016) 112.
[26] O. Mehraj, B.M. Pirzada, N.A. Mir, M.Z. Khan, S. Sabir, Appl. Surf. Sci. 387 (2016) 642.
[27] D. Xiao, K. Dai, Y. Qu, Y. Yin, H. Chen, Appl. Surf. Sci. 358 (2015) 181.
[28] B. Klahr, S. Gimenez, F. Fabregat-Santiago, T. Hamann, J. Bisquert, J. Am. Chem. Soc. 134 (2012) 4294.
[29] X. Zhou, J. Lan, G. Liu, K. Deng, Y. Yang, G. Nie, J. Yu, L. Zhi, Angew. Chem. Int. Ed. 51 (2012) 178.
[30] X. Zhou, Q. Xu, W. Lei, T. Zhang, X. Qi, G. Liu, K. Deng, J. Yu, Small 10 (2014) 674.
[31] J. Yu, J. Low, W. Xiao, P. Zhou, M. Jaroniec, J. Am. Chem. Soc. 136 (2014) 8839.
[32] T.-K. Van, H.G. Cha, C.K. Nguyen, S.-W. Kim, M.-H. Jung, Y.S. Kang, Cryst. Growth Des. 12 (2012) 862.
[33] P. Vivek, S.V. Rajender, Chem. Soc. Rev. 37 (2008) 1546.
[34] C.W. Kim, S.J. Yeob, H.-M. Cheng, Y.S. Kang, Energy Environ. Sci. 8 (2015) 3646.
[35] R. Li, H. Han, F. Zhang, D. Wang, C. Li, Energy Environ. Sci. 7 (2014) 1369.
[36] C.W. Kim, Y.S. Son, M.J. Kang, D.Y. Kim, Y.S. Kang, Adv. Energy Mater. 6 (2016) 201501754.
[37] D. Faivre, Iron Oxides From Nature to Applications, Willey-VCH Verlag-Gmbh & Co. KGaA, 2016.